High-Sensitivity and Compact Time Domain Soil Moisture Sensor Using Dispersive Phase Shifter for Complex Permittivity Measurement

Rasool Keshavarz and Negin Shariati, *Member, IEEE*

Abstract—This article presents a time domain transmissometry soil moisture sensor (TDT-SMS) using a dispersive phase shifter (DPS), consisting of an interdigital capacitor that is loaded with a stacked four-turn complementary spiral resonator (S4-CSR). Soil moisture measurement technique of the proposed sensor is based on the complex permittivity sensing property of a DPS in time domain. Soil relative permittivity which varies with its moisture content is measured by burying the DPS under a soil mass and changing its phase difference while excited with a 114-MHz sine wave (single tone). DPS output phase and magnitude are compared with the reference signal and measured with a phase/loss detector. The proposed sensor exhibits accuracy better than ±1.2% at the highest volumetric water content (VWC = 30%) for sandy-type soil. Precise design guide is developed and simulations are performed to achieve a highly sensitive sensor. The measurement results validate the accuracy of theoretical analysis and design procedure. Owning the advantages of low profile, low power consumption, and high sensitivity makes the proposed TDT-SMS a good candidate for precision farming and internet of things (IoT) systems.

Index Terms—Complement of split-ring resonator (CSRR), complex permittivity measurement, metamaterial, phase shifter, soil moisture sensor, time-domain sensor, volumetric water content (VWC).

Nomenclature

Acronym	Description
CSRR	Complement of split-ring resonator.
DPS	Dispersive phase shifter.
EH	Energy harvester.
EMTL	Embedded microstrip transmission line.
FDR	Frequency domain reflectometry.
IoT	Internet of things.
MUT	Material under test.
PW	Pulsewidth.
S_{11}	Reflection coefficient between the port impedance and the network's input impedance at Port 1.
S_{21}	Represents the power transferred from Port 1 to Port 2 of a two-port network.
S4-CSR	Stacked four-turn complementary spiral resonator.
SRR	Split-ring resonator.
TDR	Time domain reflectometry.
TDT-SMS	Time domain transmissometry soil moisture sensor.
VNA	Vector network analyzer.
VUT	Volume under test.
VWC	Volumetric water content.
WPT	Wireless power transfer.
WSNs	Wireless sensor networks.

I. Introduction

SOIL moisture is a major contributing factor in environmental challenges such as climate change and natural disasters (e.g., flooding and landslides). Soil moisture plays a key role in precision agriculture due to its effect on drainage, infiltration, and fertilization, [1], [2]. Agriculture sensors are planted in the ground at different depths to measure and transmit soil properties to a central location. In this regard, WSNs and IoT offer an optimal solution by recording necessary information at a fast rate [3], [4].

Soil sensors can be categorized as electrical and electromagnetic (EM), optical and radiometric, and electrochemical sensors [5]. Electrical and EM sensors are the most commonly used sensors in precision agriculture due to the information that they can determine as well as their robustness and low-cost design compared to other soil sensors [6]. Some EM methods are based on relationship between the real part ε' of soil permittivity ε) and VWC [7], [8]. However, $\varepsilon = \varepsilon'$ - ε'', and ε'' in moist soil is comparable with the ε' value and it should be considered in the measurement setup [9]. For instance, ε'' in sandy soil changes from 0.05 to 3.5 for VWC variation of 0%–30% at 130 MHz, and ignoring the imaginary part of the complex dielectric permittivity would degrade sensor calibration precision [10].

In terms of design methods, different EM techniques have been proposed to estimate the MUT permittivit; TDR [11], time domain transmissometry (TDT), FDR [12], remote sensing, capacitance [13], and other methods [9], [14]. Some techniques require very complicated test sets or have a limited dynamic range. For example, the FDR method estimates VWC based on a resonance frequency variation due to the soil

dielectric properties. However, this method is based on a portable VNA technology and shares many of the cumbersome calibration and usage requirements for field measurements [15].

The principle of a typical TDT technique is based on the measurement of time interval that pulse travels from one starting point on the probe to the end, while the probe is surrounded by MUT (moist soil) [16]. However, when MUT is considered dispersive, its permittivity or permeability are functions of frequency $\varepsilon(\omega)$, $\mu(\omega)$). Hence, the group velocity in dispersive material is a function of frequency [17]. This leads to inaccurate measurement of the rising/falling edges of the traveling pulse [18] which is the main drawback of typical time-domain sensors. Since moist soil is like a dispersive media, different dielectric dispersion models like Debye first order, Debye second order, Drude, Lorentz, etc., are considered to model dispersion in the moist soil [18]. Therefore, the traveling pulse along the EMTL in moist soil is degraded, leading to imprecise measurement of time-domain sensors which are excited by pulse. Additionally, pulse distortion increases in inhomogeneous measurement areas which include multiple types of soils or nonuniform VWC.

The penetration of microwave signals into a MUT is defined by the skin depth coefficient, which is a function of its dielectric properties and frequency [19]. By decreasing the operational frequency band of the sensor, the skin depth increases and leads to a larger VUT measurement. Hence, the sensor covers a greater testing area (large soil volume) which is suitable for decreasing the number of sensors in a wireless sensor network constellation. However, low-frequency sensors are bulky and have their limitations in use, implementation, maintenance, and transportation. Therefore, there is a tradeoff between choosing an optimal frequency and VUT value.

Metamaterial transmission lines (TLs) have been known to miniaturize microwave devices like filters [20], [21], couplers, and other components [22], [23]. Several types of resonators are used in the body of metamaterial TLs like SRR and its complement, CSRR. There are several configurations of SRR and CSRR such as edge-coupled SRR (EC-SRR), broadside-coupled SRR (BC-SRR), nonbianisotropic SRR (NB-SRR), double-split SRR (2-SRR), and two-turn spiral resonator (2-SR) which can be used in microstrip TLs [24].

In this article, we design, simulate, test, and implement a compact TDT-SMS based on sine wave (single tone) excitation. The proposed method, unlike pulse sensors, withstands the dispersive property of moist soil and improves the measurement accuracy. The proposed TDT-SMS consists of three main parts: reference oscillator, DPS, and phase/loss detector. In the proposed method, DPS input port is excited by a sine wave (reference oscillator), while MUT (moist soil) is poured on the DPS top layer. Hence, the phase and magnitude differences between DPS output and reference signal indicate the real and imaginary parts of MUT permittivity. Moreover, a S4-CSR structure is used on the bottom layer of DPS to miniaturize its size and realize a large phase shift in a small length. Further, on the top layer of the proposed DPS, an interdigital capacitor is used to achieve a bandpass property in the operational frequency band (114 MHz). Finally,

a commercial compact gain/loss detector (AD8302) is used to detect the phase difference and loss, which can be measured using a simple multimeter in an embedded scenario for industrial applications. In the proposed technique, the sensor is implemented without using any measurement equipment like oscilloscope, spectrum analyzer, etc. This method is capable to be used in embedded sensor scenarios and massive WSNs in field measurements.

Major contributions of this article are summarized as follows.

1) This work presents a TDT-SMS that is excited with a sine-wave instead of pulse. This technique improves the sensor accuracy compared to conventional methods.

2) The proposed sensor measures the real and imaginary parts of a MUT (moist soil), simultaneously which enhance accuracy of the sensor calibration procedure.

3) For the first time, a stacked 4-CSR in a DPS structure is designed, and the effect of equivalent circuit model components on the phase difference value is analyzed.

4) In order to cover large VUT and also to achieve a compact structure, the proposed sensor is designed at low-frequency band (114 MHz), while the size is miniaturized using an S4-CSR resonator. Theoretical analysis and investigation of commercialized products support the choice of the proposed operational frequency band.

5) From practical design and economic perspectives, achieving a large phase difference in a compact structure and measuring the phase difference and loss using a compact detector, leads to a miniaturized and low-cost soil sensor. Hence, the proposed sensor is a good candidate for integrating into various industrial sensors and IoT systems.

6) The design guide procedure for other soil types or arbitrary MUT and operational frequency bands are presented and equations are derived. Therefore, the proposed technique can be generalized and extended to other applications, as it has the capability to measure the complex permittivity of different MUTs.

7) The proposed sensor consists of two main parts: DPS as a passive structure and a phase/loss detector (AD8302) which consumes low dc power (<66 mW). Since the sensing process for soil moisture measurement takes short time (less than 1 s) and repeats sometimes during a day, the proposed system acts as a low power sensor which is suitable for field measurement in massive wireless sensor networks in precision farming or other practical scenarios.

The organization of this article is as follows: Sensor design and methodology are presented in Section II. The proposed TDT-SMS performance is validated by analytical, simulation, and measurement results in Section III. Finally, conclusions are provided in Section IV.

II. Sensor Design and Methodology

Typical time-domain soil sensors (TDR or TDT) provide an estimate of moisture content by measuring the relative permittivity in response to the soil VWC, which is determined
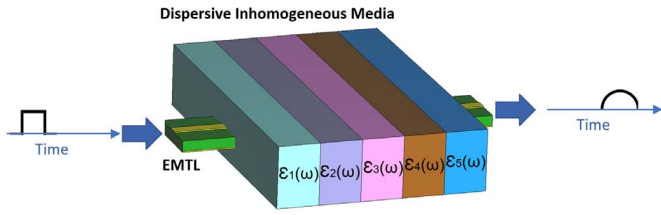
Fig. 1. Pulse distortion in a dispersive inhomogeneous media with five different materials $[\varepsilon_1(\omega), \varepsilon_2(\omega), \varepsilon_3(\omega), \varepsilon_4(\omega), \varepsilon_5(\omega)]$.

by the time an EM pulse travels in soil. The main difference between TDR and TDT is that the latter measures the time of transmission and not reflection, as TDR [16]. In this section, first, we simulate the effect of moist soil as a dispersive media on the pulse distortion in typical time-domain sensors and compare it with the proposed sine wave excitation technique. Then, the theory and design guide of a DPS as the main part of the proposed TDT-SMS will be investigated.

A. Time-Domain Sensors in Dispersive Media

In dispersive media, the permittivity or permeability of MUT is function of frequency ($\varepsilon(\omega)$, $\mu(\omega)$). Dispersion leads to a pulse distortion which can be intensified when MUT is inhomogeneous and encompasses multiple soil types and nonuniform VWC. Fig. 1 exhibits an inhomogeneous media which consists of five different materials. Moreover, since the permittivity of each material depends on frequency, this structure is a dispersive inhomogeneous media. Fig. 2 exhibits CST simulation results of a conventional EMTL, with the length of 60 cm, while excited with rectangular pulses with different pulse widths (PW = 50 ps, 450 ps, and 1 ns). The results are compared with sine wave excitation for three VWC values (10%, 20%, and 30%). In this simulation, the moist sandy dispersion model was extracted from data in [25] and then CST software is used to define a dispersive material in the simulation process as the moist soil.

According to Fig. 2(a)–(c), distortions are generated in the output wave when EMTL is excited with pulses. This degradation increases by reducing the PW. Moreover, at a higher VWC level, distortion increases, and the rising/falling edges of the pulses are not precisely detectable. However, in the single tone excitation technique using a sine wave, no distortion occurs [see Fig. 2(d)]. Therefore, since pulse distortion in dispersive and inhomogeneous media is a drawback of time-domain sensors, we propose a TDT-SMS based on the sine wave excitation technique to measure the complex permittivity of MUT (moist soil).

B. Compact DPS Design

The proposed TDT-SMS consists of three main parts: reference oscillator, DPS, and phase/loss detector (see Fig. 3). The phase and magnitude difference between the reference and phase-shifted signals are measured using a phase/loss detector, when the DPS is excited with a sine wave and surrounded by the moist soil (MUT). Measured phase and magnitude are
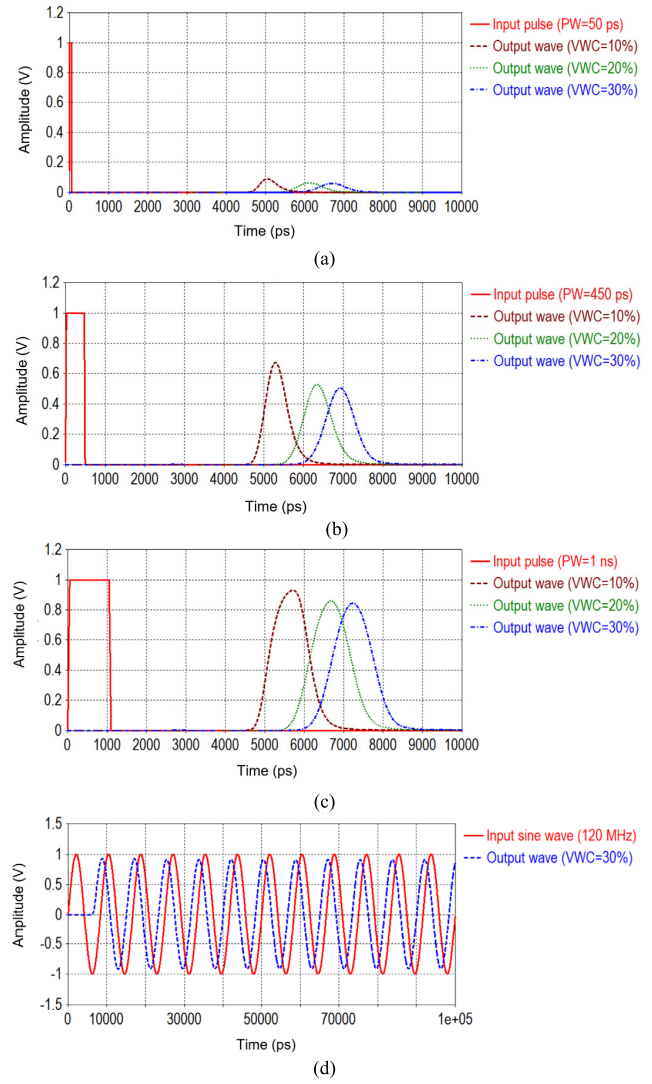

Fig. 2. Distortion in a dispersive media for pulse and sine wave excitations in different VWC values. (a) PW = 50 ps. (b) PW = 450 ps. (c) PW = 1 ns. (d) 120-MHz sine wave.
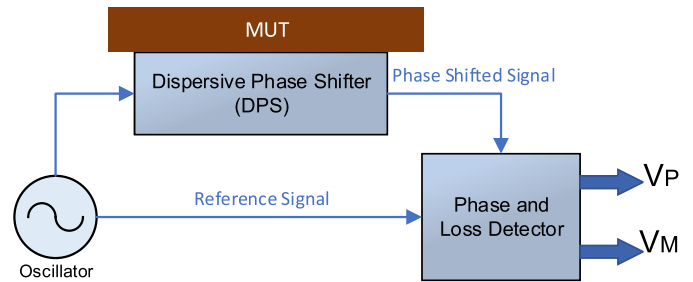

Fig. 3. Schematic of the proposed TDT-SMS based on sine wave excitation.

related to ε' and ε'', respectively, and the proposed sensor is capable to report the complex permittivity of moist soil (MUT). In this section, design theory of the proposed DPS is discussed.

There are two challenges of using a microstrip TL to realize a phase shifter in the proposed TDT-SMS under sine
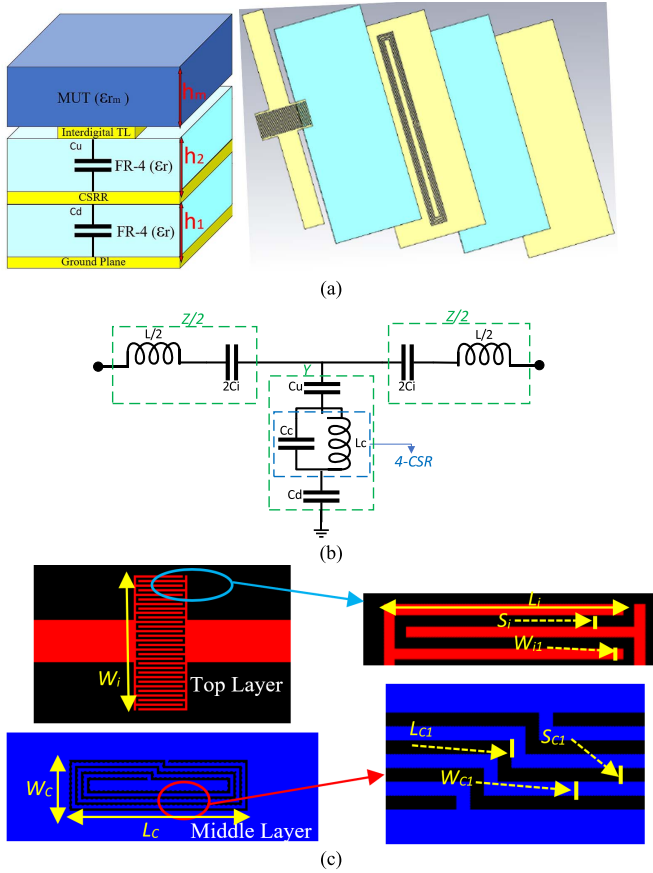
Fig. 4. Proposed TDT-SMS. (a) 3-D view of layers. (b) Equivalent circuit model. (c) Top and middle layers.

wave excitation. First, long TL is required to achieve an adequate phase shift, leading to a measurable phase difference between the output wave and reference signal. Second, the low sensitivity of conventional microstrip TL, S_M, which is the ratio of phase difference variation ($d(\Delta\emptyset)$) per unit variation of the MUT relative permittivity ($\varepsilon_{\rm rm}$) as

$$S_M = \frac{d(\Delta\emptyset)}{d(\varepsilon_{\rm rm})}. \tag{1}$$

For instance, conventional microstrip TL on FR-4 substrate with thickness of 0.6 mm exhibits 5.5-ps/mm time delay, where the phase difference at 120 MHz is around 0.23°/mm. Therefore, a length of 10 cm is required to achieve 23° phase differences (measurable value), which is not suitable for compact sensor design. Further, the S_M for this microstrip, TL is 0.023°/mm and a microstrip TL with length of 10 cm reaches $S_M = 23°$. Therefore, we propose a TDT-SMS that uses a DPS to achieve high phase difference and high sensitivity in a compact structure.

The 3-D layers schematic, equivalent circuit model, and layers of the proposed DPS are presented in Fig. 4. This structure consists of three layers: interdigital capacitor and conventional microstrip line (top layer), 4-CSR (middle layer), and ground metal cover (bottom layer), and between these metal layers are filled with the same substrate (FR-4). The middle and bottom layers form a S4-CSR which improves

the resolution of the proposed TDT-SMS and its theory is discussed in this section.

Due to the small electrical dimensions of DPS at the resonance frequency, it can be described using lumped element equivalent circuits. In the equivalent circuit in Fig. 4(b), L and C_u indicate the per-section inductance and capacitance of the top layer, C_c and L_c model the 4-CSR, C_d represents the capacitance between middle and bottom layers, and C_i denotes the series interdigital capacitance on the top layer.

The dispersion relation of the DPS is deduced from the equivalent circuit as [26]

$$\cos(\beta l) = 1 + ZY/2 \tag{2}$$

$$Z_c = \sqrt{\frac{Z}{2}\left(\frac{Z}{2} + \frac{2}{Y}\right)}. \tag{3}$$

The allowed band for backward-wave propagation in the structures occurs in the region where the characteristic impedance, Z_c, and the phase constant, βl [given by expressions (1) and (2)] are both real numbers. From [27] and considering $C_t = C_u + C_d$ as the total capacitance between layers, the upper and lower cutoff frequency bands, f_{cu} and f_{cl}, are given as

$$f_{cu} = \frac{1}{2\pi\sqrt{LC_i}}, \quad f_{cl} = \frac{\sqrt{b - \sqrt{b^2 - 4ac}}}{2\pi\sqrt{2a}} \tag{4}$$

where

$$\begin{cases} a = \mathrm{CL}L_c C_c C_i \\ b = \mathrm{CL}C_i + 8C_i L_c(C_c + C) + L_c C_c \\ c = 8C_i + C. \end{cases} \tag{5}$$

Moreover, according to the equivalent circuit model in Fig. 4(b), there are two transmission zero frequencies at $Z = \infty$ and $Y = \infty$ as

$$Z = \infty \rightarrow \frac{j\omega L}{2} + \frac{1}{2j\omega C_i} = \infty \rightarrow f_{z1} = 0 \tag{6}$$

and

$$Y = \infty \rightarrow \frac{j\omega C_t(1 - \omega^2 L_c C_c)}{1 - \omega^2 L_c(C_c + C_t)} = \infty \rightarrow f_{z2}$$

$$= \frac{1}{2\pi\sqrt{L_c(C_c + C_t)}}. \tag{7}$$

$f_{z1} = 0$ is far from the operational frequency band. However, f_{z2} can be considered very close to the lower cutoff frequency band (f_{cl}) to achieve more rejection in the out of band region. In addition, in Section III, it is shown that choosing f_{z2} very close to f_{cl} improves the sensitivity of TDT-SMS relative to changing of soil permittivity.

C. TDT-SMS Sensitivity Calculation Approach

Now, the effect of each component in the equivalent circuit model of the proposed DPS [see Fig. 4(b)] on the sensing procedure is investigated. The inductors in the DPS equivalent circuit model (L, L_c) are not impacted by the MUT permittivity, and they are approximately constant in the measurement procedure. Therefore, capacitances (C_u, C_d, C_c, and C_i) are key components in the DPS analysis.

The capacitance C_c in Fig. 4(b), corresponds to the 4-CSR structure in the middle layer. Total equivalent capacitance of the slot structure, which is the sum of series combination of capacitances in each turn for 4-CSR structure can be calculated from [28]

$$\frac{1}{C_c} = \sum_{n=1}^{N} \frac{1}{\varepsilon_0 \left(\frac{\varepsilon_r+1}{2}\right) \left[\frac{P_n t_m}{S_c} + \frac{2\pi t_m}{\ln(8t_m/P_n)}\right]} \quad (8)$$

where t_m, P_n, and S_c are metal thickness, CSRs lengths, and gap width, respectively. According to (8), C_c is not related to the MUT permittivity, and it can be ignored in the sensitivity calculation of the proposed TDT-SMS.

Moreover, the calculation of C_u and C_d is more straightforward and can be defined as the capacitance between two metal parallel plates [see Fig. 4(a)]. In C_d, if the narrow slots on the middle layer (4-CSR layer) are ignored, the bottom substrate is approximately surrounded between two metal plates (4-CSR layer and ground plane) and isolated from MUT and ε_m variations. Moreover, the simulated and measured results in Section III confirm the assumption of ignoring narrow slots on the middle layer in C_d calculation.

However, in C_u [see Fig. 4(a)], the upper substrate is limited between the middle layer and interdigital/microstrip TL structure on the top layer which is embedded inside a moist soil (MUT). In this case, there are fringing fields on the top layer, and the effective area of the top plate changes relative to ε_m variation. Therefore, the values of C_d and C_u can be calculated as [29]

$$C_d = \varepsilon_0 \varepsilon_r \frac{A_d}{h_d} \quad (9)$$

$$C_u = \varepsilon_0 \varepsilon_r \frac{A'_u}{h_u} \quad (10)$$

where A_d, h_d, and h_u are physical area of the bottom ground layer, thicknesses of the lower and upper substrates, respectively, and

$$A'_u = a \cdot (b + 2\Delta L) = A_u + 2a\,\Delta L \quad (11)$$

where a, b, and A'_u are physical width, length, and effective area of the top layer, respectively, considering effective length increment, ΔL, as [29]

$$\Delta L = 0.412h \left[\frac{(\varepsilon_{reff} + 0.3)(h_u + 0.3)}{(\varepsilon_{reff} - 0.258)(a/h_u + 0.8)}\right]. \quad (12)$$

Effective permittivity (ε_{reff}) of a microstrip line that is buried under a MUT can be expressed as [30]

$$\varepsilon_{eff} = \varepsilon_0 \left[(\varepsilon_r + \varepsilon_m)/2 + \left((\varepsilon_r - \varepsilon_m)/2\sqrt{1 + 12\frac{h_u}{a}}\right)\right]$$
$$\text{if } h_m \gg h_u \quad (13)$$

where h_m is MUT thickness. Therefore, according to (9)–(13), C_d and C_u are calculated and the impact of MUT permittivity (ε_m) on them is considered.

The fourth capacitance in the SMS equivalent circuit model is C_i which is related to the interdigital capacitance on the
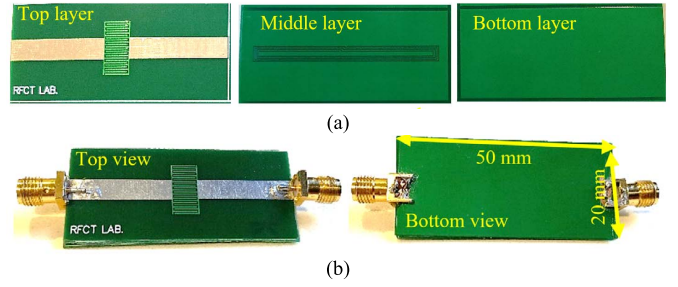

Fig. 5. Prototype of the proposed DPS. (a) Top layer, middle layer, and bottom layer. (b) Assembled DPS (top and bottom view).

top layer. Several formulas to calculate this capacitance are presented and we used the following one [31]:

$$C_i(\text{pF}) = (\varepsilon_{reff} + 1)l_i[(N - 3)A_1 + A_2] \quad (14)$$

where

$$A_1 = 4.409\tanh\left[0.55\left(\frac{h_u}{W_i}\right)^{0.45}\right],$$

$$A_2 = 9.92\tanh\left[0.52\left(\frac{h_u}{W_i}\right)^{0.5}\right]. \quad (15)$$

Finally, according to the investigation of capacitances in the equivalent circuit model [see Fig. 4(b)], sensitivity of the proposed DPS (S_{DPS}) relative to ε_{rm} variation is derived as

$$S_{DPS} = \frac{d(\Delta \varnothing)}{d\varepsilon_{rm}} = \left(\frac{d(\Delta \varnothing)}{dC_u} \times \frac{dC_u}{d\varepsilon_{rm}}\right) + \left(\frac{d(\Delta \varnothing)}{dC_i} \times \frac{dC_i}{d\varepsilon_{rm}}\right). \quad (16)$$

As mentioned in this section, ε_{rm} variation cannot impact the other components in the equivalent circuit model in Fig. 4(b) (C_d, C_c, L_c, and L). Hence, we ignored these components in the sensitivity equation (15). In addition, the analytical calculation of (15) is complicated, so we use numerical solutions in MATLAB.

III. SIMULATION, MEASUREMENT, AND DISCUSSION

To demonstrate the functionality of the proposed TDT_SMS, DPS is designed, simulated, and optimized using CST simulator. Then, DPS is fabricated on low-cost FR-4 substrate with $\varepsilon_r = 4.3$, thickness of $h_1 = h_2 = 0.6$ mm, and a dissipation factor of 0.0037 at 120 MHz. Copper thicknesses of 35 μm were created for printing top, middle, and bottom metal layers (see Fig. 5). According to the design procedure discussed in Section II, the proposed TDT-SMS dimension is derived (see Table I), optimum values of the DPS equivalent circuit model in the unloaded state are calculated (see Table II), and the layout is extracted using equations in [30].

The scattering (S)-parameters allow to accurately describe the input–output relationships between ports, and hence the properties of the proposed DPS as a two-port network [31]. Theoretical, simulated, and measured S_{21} results of the unloaded DPS as a two-port network are presented in Fig. 6 which are in a great agreement. DPS exhibits in-band

TABLE I
DIMENSION OF THE DPS

L_i (mm)	W_i (mm)	S_i (mm)	W_{il} (mm)	L_C (mm)	W_C (mm)	L_{Cl} (mm)	S_{Cl} (mm)	W_{Cl} (mm)
5.6	17.4	0.2	0.2	44.5	3.7	0.2	0.2	0.2

TABLE II
VALUES OF THE EQUIVALENT CIRCUIT MODEL OF DPS

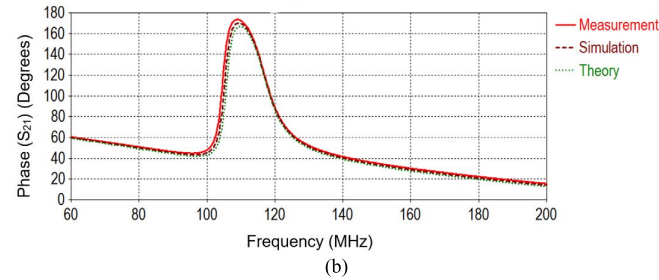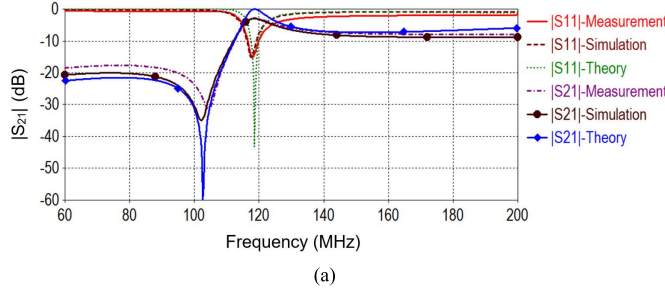| L (nH)	C_i (pF)	C_u (pF)	C_d (pF)	C_c (pF)	L_c (nH)
1.5	1.2	14.1	15.9	7.8	17.2

Fig. 6. (a) Theoretical, simulated, and measured results of unloaded sensor ($\varepsilon_m = 1$). (a) $|S_{11}|$ and $|S_{21}|$. (b) phase (S_{21}), versus frequency.

TABLE III
DIELECTRIC CONSTANT VALUES AS A FUNCTION OF VWC FOR SAND AROUND 130 MHz [24]

VWC (%)	0	5	10	15	20	25	30
ε_m'	2.5	6	8	14.5	18	21	23.5
ε_m''	0.05	0.5	0.9	1.8	2.5	3.1	3.5

insertion loss of around 3 dB, and 3-dB passband range from 114 to 135 MHz. As mentioned in Section II, there is a zero-transfer frequency near the lower cutoff frequency band at 103 MHz.

A. DPS Simulation and Measurement Results Versus VWC

Several relations between soil moisture content and soil dielectric constant have been proposed. Table III presents the real and imaginary parts of the dielectric constant values as a function of VWC around 130 MHz [25]. After validating the proposed sensor performance in the unloaded state (see Fig. 6), the structure has been embedded into the sandy soil with different VWC. Different soil VWC levels have been achieved based on that has been released by the Department of Sustainable Natural Resources NSW Australia [25]. First,
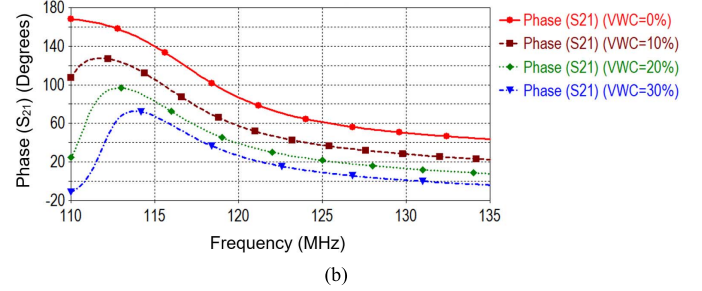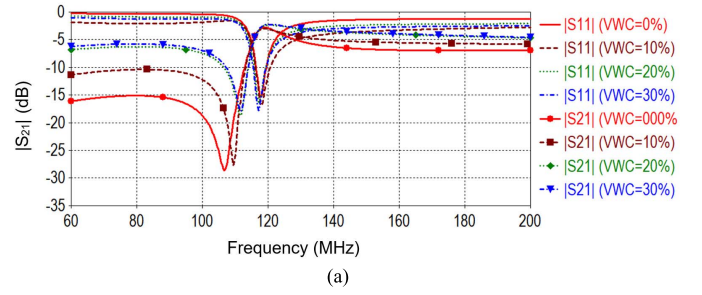

Fig. 7. Measurement results of the proposed DPS at four different values of VWC (0%, 10%, 20%, 30%) for sandy soil. (a) $|S_{11}|$ and $|S_{21}|$. (b) Phase difference (phase shift).

the sand has been put in the oven to dry it. Then, the water has been added to provide sand with 5%, 10%, 15%, 20%, 25%, and 30% VWC levels as

$$\text{VWC}(\%) = \frac{W_2}{W_1 + W_2} \times 100 \qquad (17)$$

where W_1 and W_2 are the weights of dried soil and added water, respectively. Furthermore, we measured performance of the proposed sensor in five trials for each VWC value.

The DPS was measured using a VNA (VNA-ZVA40). Fig. 7 shows the measured S-parameters results of the proposed DPS versus sandy soil with VWC of 0%, 10%, 20%, and 30%. According to Fig. 7(a), the proposed sensor operates as a bandpass filter over 114–125 MHz. By increasing the VWC value of MUT from 0% to 30%, zero frequency, lower and upper cutoff frequency bands increase. Further, the measured insertion loss of the DPS at the operational frequency bands is better than 3 dB. Fig. 7(b) demonstrates the measured results of phase difference (phase shift). It is demonstrated that each phase difference curve, which is related to a specific VWC value, has a unique pattern. This property is used to measure the VWC of soil in Section III-C.

B. DPS Sensitivity Analysis Results

In this section, the sensitivity simulation results of the proposed DPS that was investigated in Section II-B, are presented. Effective length increment, ΔL, of the top layer versus the MUT permittivity is presented in Fig. 8(a), while DPS is embedded in MUT. As it is shown, ΔL decreases from 270 to 250 μm due to ε_{rm} variation (1–24). Fig. 8(b) exhibits theoretical calculation results of C_u and C_i versus the MUT permittivity (ε_{rm}), based on effective ΔL value [see (9) and (13)]. According to this figure, when ε_{rm} changes from 1 to 24, maximum variations of C_u and C_i are 15 and
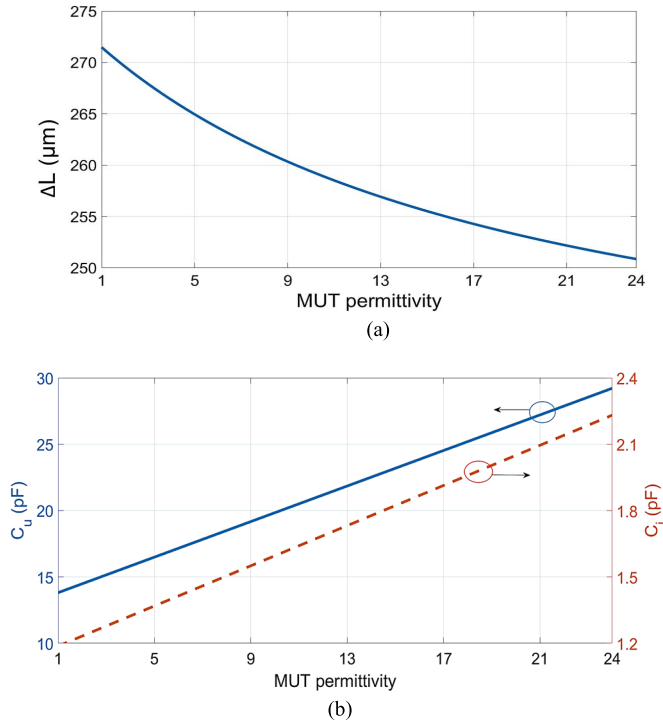
Fig. 8. (a) Effective length increment, ΔL, of the DPS top layer. (b) Theoretically calculated values of C_u and C_i capacitances, versus MUT permittivity (ε_{rm}).
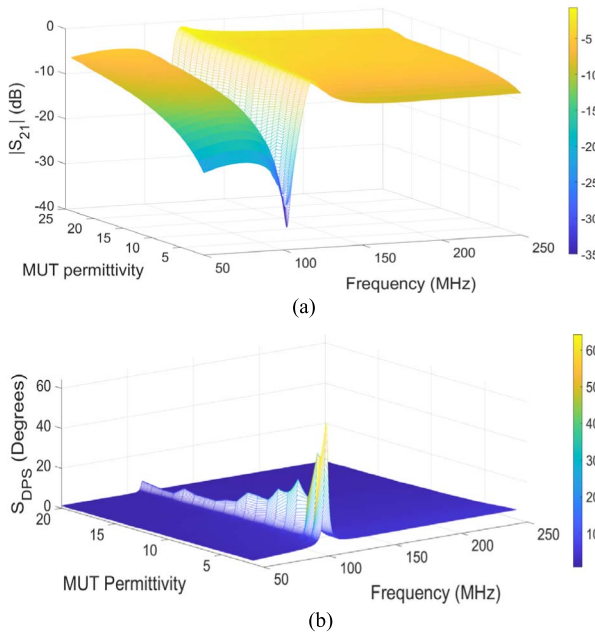

Fig. 9. Theoretical results of the proposed DPS versus frequency and MUT permittivity (ε_{rm}). (a) $|S_{21}|$. (b) DPS sensitivity (S_{DPS}).

1 pF, respectively. Hence, C_u is the most important component in the DPS system to achieve highly sensitive TDT-SMS.

Fig. 9(a) presents simulated $|S_{21}|$ of the proposed DPS versus frequency and MUT permittivity. DPS insertion loss is approximately 3 dB in the passband range when ε_{rm} changes from 1 to 24. Furthermore, rejection at the zero-transfer

frequency (near the lower cutoff frequency band) decreases as MUT permittivity increases.

Now, in the sine wave (single tone) excitation scenario, we find an optimum frequency in the passband and excite the DPS at this frequency to achieve high sensitivity, related to the MUT permittivity variation. In this regard, according to sensitivity equation (15), Fig. 9(b) presents the numerical solution of this equation in MATLAB software. This figure shows that, at a fixed operational frequency band, the DPS sensitivity (S_{DPS}) decreases as MUT permittivity increases, while the maximum sensitivity occurs around the lower cutoff frequency band of DPS. For instance, the sensitivity values at 114 MHz for $\varepsilon_{rm} = 5, 10, 15$, and 20 are around 30°, 16°, 8°, and 7°, respectively. Therefore, we select 114 MHz as the optimum frequency of the sine wave in the single tone excitation scenario.

According to Fig. 9(b), in the worst case scenario the DPS sensitivity at $\varepsilon_m = 23.5(\text{VWC} = 30\%)$ is $S_{DPS} = (d(\Delta \emptyset)/d\varepsilon_{rm}) = 7°$ and based on the measured data in [25], $(d(\text{VWC}\%)/d\varepsilon_{rm}) = 2$.

Hence, for the proposed DPS, the phase difference variation related to VWC is calculated as

$$\frac{d(\Delta \emptyset)}{d(\text{VWC}\%)} = 3.5°. \quad (18)$$

Therefore, according to (18), $\Delta \emptyset = 3.5°$ must be detectable using phase/loss detector to achieve 1% resolution in VWC. This total resolution of the proposed technique is investigated in Section III-C.

C. Embedded Realization of TDT-SMS

In the proposed TDT-SMS, phase and amplitude differences between the reference and phase-shifted signals are detected using a phase/loss detector (see Fig. 3). The measured phase and amplitude differences are related to the real and imaginary parts of MUT permittivity, respectively. In the embedded scenario, the detector converts these differences to output voltages V_P and V_M which are related to phase differences and loss, respectively, and can be measured using a simple multimeter. We used AD8302 which is a fully integrated system for measuring phase and loss [32]. Two outputs of AD8302, V_M and V_P, provide an accurate measurement of loss over a ±30-dB range scaled to 30 mV/dB, and phase over a 0°–180° range scaled to 10 mV/°. According to the AD8302 datasheet, at 100 MHz, the accuracy of measuring phase difference, from 30° to 150°, is better than 0.1° and the accuracy of loss measurement from −25 to 0 dB, is 0.1 dB [32]. Therefore, the loss and phase measurement region should be considered in this area to achieve a high accuracy sensor.

Fig. 10(a) shows the block diagram of the measurement setup. A two-channel Vector Signal Generator (SMW200A) is used as the reference signal generator. In order to verify the sensor accuracy, an oscilloscope (RTO2044) is used to measure phase-shifted and reference signals and verify the V_P and V_M results, which were measured using AD8302 and multimeter (HMC8012). Finally, we used two power splitters (ZFSC-2-4) to organize measuring and verification procedures, simultaneously. Fig. 10(b)–(d) shows the measurement setup
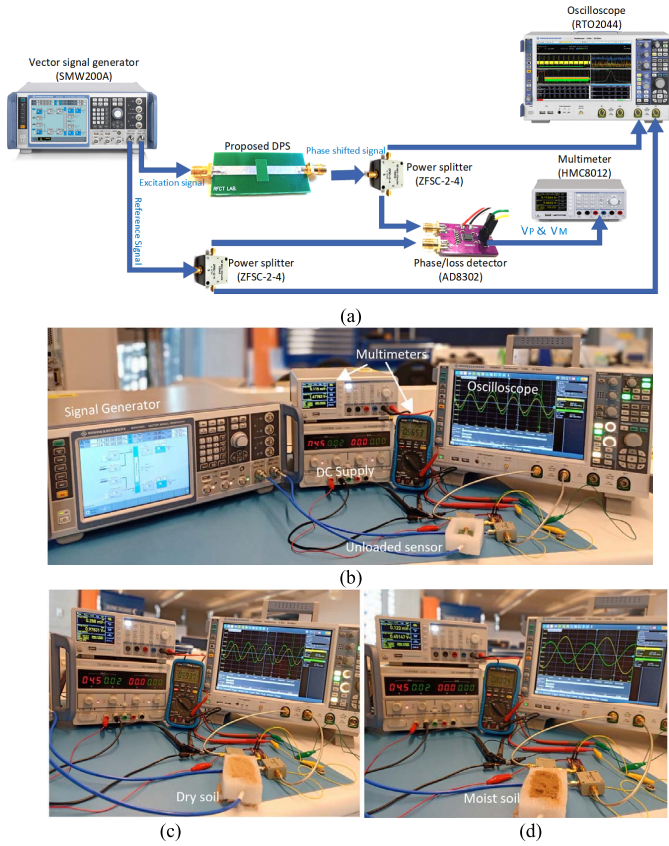
Fig. 10. (a) Measurement setup of embedded TDT-SMS and required equipment, (b) unloaded, (c) dry soil, and (d) moist soil.

Fig. 11. Testing process of permittivity and VWC for moist soil.

in unloaded, dry soil, and moist soil cases, respectively. Before starting the measurement process, the setup is calibrated considering the loss and phase differences of all signal directions.

In the proposed sensing method, the VWC measurement is based on the permittivity detection technique of moist soil and then relating the measured permittivity to VWC of soil. Therefore, the resolution of VWC measurement depends on the permittivity measurement resolution. According to Fig. 10(a), since the phase difference of DPS output signal is measured relative to the reference oscillator using phase/loss detector, the AD8302 resolution determines the resolution of testing parameter. From (18), the accuracy of measuring phase difference using AD8302 is 0.1°, and the total resolution of the proposed sensing technique is

$$\Delta\emptyset > 0.1° \rightarrow \Delta(\text{VWC\%}) = 0.03\%. \qquad (19)$$

However, 0.03% is a theoretical value for resolution and in the real measurement setup, there are several noise sources and interference that can degrade the resolution value. According to the commercialized soil moisture sensors [33], VWC = 1% is an acceptable value and the proposed sensor meets this amount.

There are three stages of testing permittivity and VWC in the proposed technique as shown in Fig. 11. According to Table III and existing data in [25], nominal values are provided for real and imaginary parts of soil permittivity relevant to each VWC. At this stage, we assigned the nominal values of
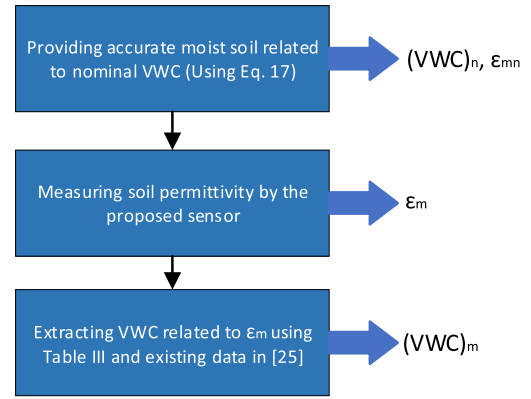
permittivity (ε_{mn}) and $(\text{VWC})_n$ to the produced moist soil. Then, the measured values of soil permittivity are compared with the nominal values and estimation error is defined as

$$\text{Estimation error} = \frac{|\varepsilon_m - \varepsilon_{mn}|}{\varepsilon_{mn}} \times 100. \qquad (20)$$

Fig. 12 demonstrates the measured results of testing setup in Fig. 10 when TDT-SMS was excited with 114 MHz sine wave (the results were recorded in five trials). Fig. 12(a) and (b) shows the extracted real and imaginary parts of the MUT (sandy soil) in VWC of 0%, 5%, 10%, 15%, 20%, 25%, and 30%. These figures exhibit an average error of the measured real and imaginary parts 3.5% and 11%, respectively. After measuring real and imaginary parts of soil permittivity, Fig. 12(a) and (b), the soil moisture value (VWC) is calculated using data in Table III. According to Fig. 12(c), the estimation error is less than ±0.3%, ±0.6%, ±0.8%, and ±1.2% at 0%, 10%, 20%, and 30% VWC of sandy soil, respectively. The achieved measurement results confirm the accuracy of the proposed sensing technique and design procedure.

Table IV compares the performance of the proposed sensor with other reported sensors. Moreover, to provide a fair comparison with previously published articles in this table, the references are compared with the proposed technique in terms of permittivity which is a general parameter to compare different sensors, regardless of their applications. Furthermore, in terms of different compositions of soil and its effect on the permittivity measurement accuracy, we consider sandy soil type in our study so that the permittivity of various dried sandy soil occupied a narrow range of values (less than 0.3 variation in the permittivity) around operating frequency range (114 MHz) and it confirms the reasonability of the comparison process.

From Table IV, it is evident that, with 3.5% measured error of the real permittivity, the proposed sensor exhibits higher accuracy in a broad range of permittivity (1–23.5) in comparison with other works. Moreover, most of reported works are based on FDR technique which has several challenges in real applications and field measurements. This comparison proves the usefulness of our proposed TDT-SMS sensor for precision farming applications.

TABLE IV
COMPARISON TABLE

| Ref.	Technique	Frequency Band (GHz)	Sensitivity in Permittivity Measurement	Measured Permittivity Range	Permittivity Measurement Error (%)	Application
[35]	FDR	1.7	33.3 MHz	1~10.2	NA	Comparator functionality
[36]	FDR	4.5	60 MHz	4.4	4.3	NA
[37]	FDR	2.7	NA	10.2	7.6	NA
[38]	FDR	5.5	3.34 MHz	30	NA	Microfluid
[11]	TDR (Pulse)	0.01~1	NA	1~20 (real), 1~7 (imaginary)	5 (non dispersive), 20 (dispersive)	Soil moisture
This Work	TDT (Single tone)	0.114	7^0	1~23.5 (real), 0.1~4 (imaginary)	3.5 (non dispersive), 3.5 (dispersive)	Soil moisture
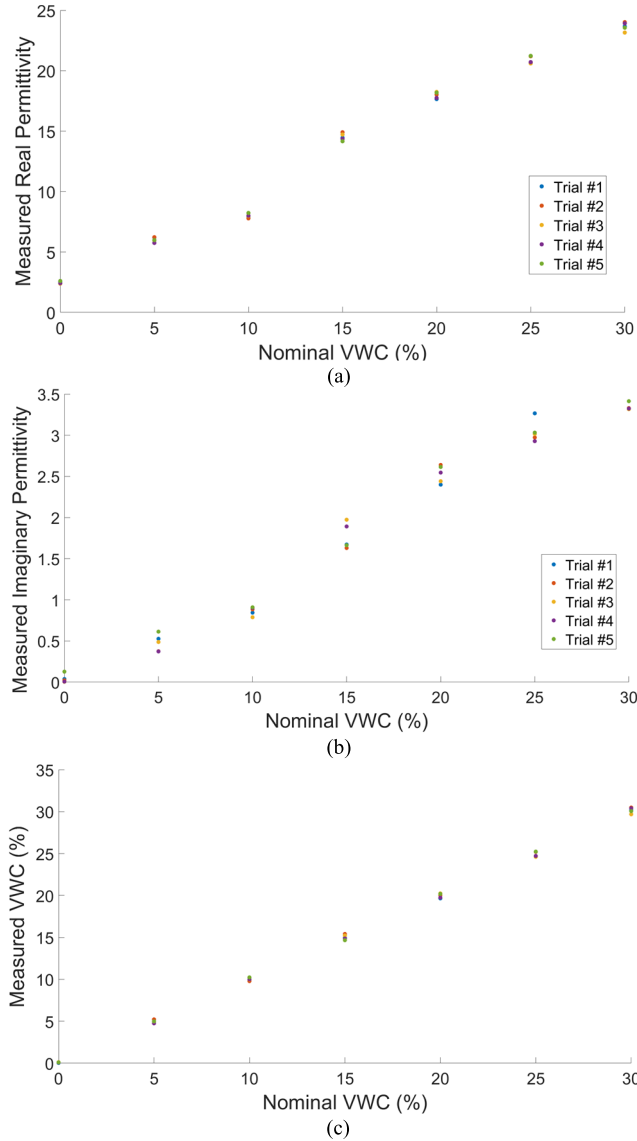
Fig. 12. Measured results of sandy soil for different nominal VWC values in five trials. (a) Real permittivity. (b) Imaginary permittivity. (c) VWC.

IV. CONCLUSION

This work demonstrates the design, simulation, and measurement of a highly sensitive and compact TDT-SMS based on a DPS. The proposed sensor achieved high phase shift value, low profile, low cost, simple usage, and high sensitivity for different VWC values. To achieve a low profile DPS, an interdigital capacitor was used on the top layer and stacked 4-CSR on the bottom layer of the proposed DPS. The TDT-SMS is excited with a 114-MHz sine wave as the reference oscillator. By measuring the phase difference and loss between the reference and phase-shifted signals, real and imaginary parts of the soil permittivity were measured, respectively, and VWC was extracted. Accuracy of $\pm 1.2\%$ at VWC of 30% was achieved (worst case scenario for sensitivity), which is very suitable in sensing applications. Furthermore, the developed design guideline of TDT-SMS can be used in the measuring process of different materials under test (MUTs). Hence, the proposed time-domain technique can be adapted to different scenarios and applications. It is the scope of our future work to design an embedded low-power soil moisture sensor and eliminate any need for testing equipment. In addition, EH or WPT devices [22], [33], [34], can be integrated with the proposed sensor to realize a self-sustainable sensor (S^3) that is of paramount importance in field measurements for precision agriculture and industrial applications.

REFERENCES

[1] W. Wagner, K. Scipal, C. Pathe, D. Gerten, W. Lucht, and B. Rudolf, "Evaluation of the agreement between the first global remotely sensed soil moisture data with model and precipitation data," *J. Geophys. Res., Atmos.*, vol. 108, no. D19, p. 4611, Oct. 2003.

[2] J. Siden, X. Zeng, T. Unander, A. Koptyug, and H.-E. Nilsson, "Remote moisture sensing utilizing ordinary RFID tags," in *Proc. IEEE SENSORS*, Atlanta, GA, USA, Oct. 2007, pp. 308–311.

[3] N. Khalid, R. Mirzavand, H. Saghlatoon, M. M. Honari, A. K. Iyer, and P. Mousavi, "A battery-less RFID sensor architecture with distance ambiguity resolution for smart home IoT applications," *IEEE Internet Things J.*, early access, Jul. 6, 2021, doi: 10.1109/JIOT.2021.3095136.

[4] I. Zhou *et al.*, "Internet of Things 2.0: Concepts, applications, and future directions," *IEEE Access*, vol. 9, pp. 70961–71012, 2021.

[5] S. U. S. Lekshmi, D. N. Singh, and M. S. Baghini, "A critical review of soil moisture measurement," *Measurement*, vol. 54, pp. 92–105, Aug. 2014.

[6] V. I. Adamchuk, J. W. Hummel, M. T. Morgan, and S. K. Upadhyaya, "On-the-go soil sensors for precision agriculture," *Comput. Electron. Agricult.*, vol. 44, no. 1, pp. 71–91, 2004.

[7] M. P. Goswami, B. Montazer, and U. Sarma, "Design and characterization of a fringing field capacitive soil moisture sensor," *IEEE Trans. Instrum. Meas.*, vol. 68, no. 3, pp. 913–922, Mar. 2019.

[8] I. Cappelli *et al.*, "Battery-less HF RFID sensor tag for soil moisture measurements," *IEEE Trans. Instrum. Meas.*, vol. 70, pp. 1–13, 2021.

[9] E. T. Engman and N. Chauhan, "Status of microwave soil moisture measurements with remote sensing," *Remote Sens. Environ.*, vol. 51, no. 1, pp. 189–198, Jan. 1995.

[10] G. C. Topp, S. Zegelin, and I. White, "Impacts of the real and imaginary components of relative permittivity on time domain reflectometry measurements in soils," *Soil Sci. Soc. Amer. J.*, vol. 64, no. 4, pp. 1244–1252, Jul. 2000.

[11] C.-P. Lin, Y. J. Ngui, and C.-H. Lin, "Multiple reflection analysis of TDR signal for complex dielectric spectroscopy," *IEEE Trans. Instrum. Meas.*, vol. 67, no. 11, pp. 2649–2661, Nov. 2018.

[12] H.-J. Lee and J.-G. Yook, "Biosensing using split-ring resonators at microwave regime," *Appl. Phys. Lett.*, vol. 92, no. 25, Jun. 2008, Art. no. 254103.

[13] M. J. Oates, A. Fernández-López, M. Ferrández-Villena, and A. Ruiz-Canales, "Temperature compensation in a low cost frequency domain (capacitance based) soil moisture sensor," *Agricult. Water Manage.*, vol. 183, no. 1, pp. 86–93, Mar. 2017.

[14] R. Keshavarz, J. Lipman, D. M. M.-P. Schreurs, and N. Shariati, "Highly sensitive differential microwave sensor for soil moisture measurement," *IEEE Sensors J.*, vol. 21, no. 24, pp. 27458–27464, Dec. 2021, doi: 10.1109/JSEN.2021.3125718.

[15] P. Snógren, M. Berglund, and A. Persson, "Combined pressure and flow sensor integrated in a split-ring resonator microplasma source," *Appl. Phys. Lett.*, vol. 109, no. 17, Oct. 2016, Art. no. 173508.

[16] T. B. Wilson *et al.*, "Evaluating time domain reflectometry and coaxial impedance sensors for soil observations by the U.S. Climate reference network," *Vadose Zone J.*, vol. 19, no. 1, Jan. 2020, Art. no. e20013.

[17] P. Rulikowski and J. Barrett, "Ultra-wideband pulse shaping using lossy and dispersive nonuniform transmission lines," *IEEE Trans. Microw. Theory Techn.*, vol. 59, no. 10, pp. 2431–2440, Oct. 2011.

[18] I. Giannakis and A. Giannopoulos, "A novel piecewise linear recursive convolution approach for dispersive media using the finite-difference time-domain method," *IEEE Trans. Antennas Propag.*, vol. 62, no. 5, pp. 2669–2678, May 2014.

[19] D. Pozar, *Microwave Engineering*. Hoboken, NJ, USA: Wiley, 2011.

[20] R. Keshavarz and N. Shariati, "Low profile metamaterial band-pass filter loaded with 4-turn complementary spiral resonator for WPT applications," in *Proc. 27th IEEE Int. Conf. Electron., Circuits Syst. (ICECS)*, Glasgow, U.K., Nov. 2020, pp. 1–4.

[21] R. Keshavarz, Y. Miyanaga, M. Yamamoto, T. Hikage, and N. Shariati, "Metamaterial-inspired quad-band notch filter for LTE band receivers and WPT applications," in *Proc. IEEE 33rd Gen. Assem. Sci. Symp. Int. Union Radio Sci.*, Rome, Italy, Sep. 2020, pp. 1–4.

[22] R. Keshavarz and N. Shariati, "Highly sensitive and compact quad-band ambient RF energy harvester," *IEEE Trans. Ind. Electron.*, early access, May 3, 2021, doi: 10.1109/TIE.2021.3075888.

[23] R. Keshavarz, A. Mohammadi, and A. Abdipour, "A quad-band distributed amplifier with E-CRLH transmission line," *IEEE Trans. Microw. Theory Techn.*, vol. 61, no. 12, pp. 4188–4194, Dec. 2013.

[24] M. Gil, J. Bonache, and F. Martin, "Metamaterial filters: A review," *Metamaterials*, vol. 2, no. 4, pp. 186–197, 2008.

[25] J. Cihlar and F. T. Ulaby, "Dielectric properties of soils as a function of moisture content," NASA, Huston, TX, USA, Tech. Rep. 177-47, 1974.

[26] C. Caloz, "Dual composite right/left-handed (D-CRLH) transmission line metamaterial," *IEEE Microw. Wireless Compon. Lett.*, vol. 16, no. 11, pp. 585–587, Nov. 2006.

[27] F. Martín, J. Bonache, F. Falcone, M. Sorolla, and R. Marqués, "Split ring resonator-based left-handed coplanar waveguide," *Appl. Phys. Lett.*, vol. 83, no. 22, pp. 4652–4654, Dec. 2003.

[28] O. Sydoruk, E. Tatartschuk, E. Shamonina, and L. Solymar, "Analytical formulation for the resonant frequency of split rings," *J. Appl. Phys.*, vol. 105, no. 1, 2009, Art. no. 014903.

[29] A. Elrashidi, K. Elleithy, and H. Bajwa, "The fringing and resonance frequency of cylindrical microstrip printed antenna as a function of curvature," *EURASIP J. Wireless Commun. Netw.*, vol. 3, no. 2, pp. 1–10, 2011.

[30] R. Marqués, F. Martín, and M. Sorolla, *Metamaterials With Negative Parameters: Theory, Design, and Microwave Applications*. Hoboken, NJ, USA: Wiley, 2007.

[31] I. Bahl, *Lumped Elements for RF and Microwave Circuits*. Norwood, MA, USA: Artech House, 2003.

[32] *AnalogDevice*. Accessed: Aug. 2021. [Online]. Available: https://www.analog.com/en/products/ad8302.html

[33] *Australia*. Accessed: Aug. 2021. [Online]. Available: https://www.ictinternational.com

[34] N. Shariati, W. S. T. Rowe, J. R. Scott, and K. Ghorbani, "Multi-service highly sensitive rectifier for enhanced RF energy scavenging," *Sci. Rep.*, vol. 5, no. 1, p. 9655, Sep. 2015.

[35] L. Su, J. Mata-Contreras, P. Vélez, and F. Martín, "Splitter/combiner microstrip sections loaded with pairs of complementary split ring resonators (CSRRs): Modeling and optimization for differential sensing applications," *IEEE Trans. Microw. Theory Techn.*, vol. 64, no. 12, pp. 4362–4370, Dec. 2016.

[36] C.-L. Yang, C.-S. Lee, K.-W. Chen, and K.-Z. Chen, "Noncontact measurement of complex permittivity and thickness by using planar resonators," *IEEE Trans. Microw. Theory Techn.*, vol. 64, no. 1, pp. 247–257, Jan. 2016.

[37] C.-S. Lee and C.-L. Yang, "Complementary split-ring resonators for measuring dielectric constants and loss tangents," *IEEE Microw. Wireless Compon. Lett.*, vol. 24, no. 8, pp. 563–565, Aug. 2014.

[38] A. Salim and S. Lim, "Complementary split-ring resonator-loaded microfluidic ethanol chemical sensor," *Sensors*, vol. 16, no. 11, p. 1802, Oct. 2016.

Rasool Keshavarz was born in Shiraz, Iran, in 1986. He received the Ph.D. degree in telecommunications engineering from the Amirkabir University of Technology, Tehran, Iran, in 2017.

He is currently working as a Post-Doctoral Research Associate with the Radio Frequency and Communication Technologies (RFCT) Research Laboratory, University of Technology Sydney, Ultimo, NSW, Australia. His main research interests include RF and microwave circuit and system design, sensors, antenna design, wireless power transfer (WPT), and RF energy harvesting (EH).

Negin Shariati (Member, IEEE) received the Ph.D. degree in electrical-electronic and communication technologies from the Royal Melbourne Institute of Technology (RMIT), Melbourne, VIC, Australia, in 2016.

She has worked in industry as an Electrical-Electronic Engineer from 2009 to 2012. She is currently a Senior Lecturer with the Faculty of Engineering and IT, School of Electrical and Data Engineering, University of Technology Sydney (UTS), Ultimo, NSW, Australia. She has established the state-of-the-art RF and Communication Technologies (RFCT) Research Laboratory, UTS, in 2018, where she is currently the Co-Director and leads research and development in RF-electronics, sustainable sensing, the low-power Internet of Things, and energy harvesting. She leads the Sensing Innovations Constellation at Food Agility Corporative Research Centre (CRC), enabling new innovations in agriculture technologies by focusing on three key interrelated streams: sensing, power, and connectivity. In 2018, she has held a joint appointment as a Senior Lecturer at Hokkaido University, Sapporo, Japan, externally engaging with research and teaching activities in Japan. She attracted over one million dollar worth of research funding across a number of CRC and industry projects, where she has taken the lead CI role and also contributed as a member of the CI Team. Her research interests include microwave circuits and systems, RF energy harvesting, the low-power IoT, simultaneous wireless information and power transfer, wireless sensor networks, antenna, and AgTech.